Validation of ERMES 20.0 finite element code for JET A2 antennas coupling studies

Validation of ERMES 20.0 finite element code for JET A2 antennas coupling studies

Ruben Otin[1,*], *Daniele* Milanesio[2], *Philippe* Jacquet[1], and *Igor* Monakhov[1]

[1]United Kingdom Atomic Energy Authority (UKAEA), Culham Science Centre, OX14 3DB, UK
[2]Politecnico di Torino, Torino, Italy

Abstract. This study presents the validation of the finite element code ERMES 20.0, benchmarked against the well-established method-of-moments code TOPICA. The simulations focus on Ion Cyclotron Resonance Heating (ICRH) coupling for the JET A2 antennas. Validation is performed by comparing two key metrics: the scattering parameter matrix (S-matrix) and the electric field distribution in front of the antenna. These parameters are critical for assessing ICRH antenna-plasma coupling efficiency and understanding interactions with plasma-facing components. The results show a strong agreement between ERMES 20.0 and TOPICA, confirming the accuracy and reliability of the finite element approach. This comparative analysis highlights the capability of ERMES 20.0 to support advanced modeling of sheath rectification and wave–edge plasma interactions, which are central phenomena in ICRH system design and optimization.

1 Introduction

Ion Cyclotron Resonance Heating (ICRH) remains a cornerstone technique for auxiliary heating in magnetic confinement fusion devices [1, 2]. Its effectiveness critically depends on the efficient coupling of Radio-Frequency (RF) power to the plasma and the mitigation of parasitic effects in the Scrape-Off Layer (SOL), such as sheath rectification [3]. Accurate numerical modeling of the antenna–plasma interaction is essential for optimizing antenna design, predicting coupling performance, and understanding SOL phenomena that can limit ICRH heating power and overall fusion performance.

To address this need, the open-source Finite Element Method (FEM) code ERMES 20.0 [4] has been adapted to provide a robust and flexible approach for handling the complex geometries and boundary conditions inherent to ICRH antenna–plasma systems. This paper presents a validation of ERMES 20.0, benchmarked against the well-established Method-of-Moments (MoM) code TOPICA [5]. Simulations are carried out in the context of ICRH coupling studies for the JET A2 antennas [6, 7], which represent a well-characterized and experimentally relevant test case.

The validation focuses on comparing key physical quantities relevant to ICRH performance, such as the scattering parameters matrix (S-matrix) and the electric field distribution in the region immediately in front of the antenna. These metrics are directly linked to coupling efficiency and SOL effects, which are critical for understanding both power deposition and plasma-wall interactions.

This paper is structured as follows: Section 2 describes the simulation setup used as a benchmark for both ERMES and TOPICA. Sections 3 and 4 present the numerical approaches, boundary conditions, and distinctive features of each code. Section 5 shows and discusses the validation results, while section 6 summarizes the findings and offers concluding remarks and directions for future work.

2 Benchmark description

A common benchmark configuration based on two JET pulses, including measured plasma profiles and a realistic CAD model of the JET A2 antenna, was established to validate ERMES 20.0 against TOPICA. The 3D model of the JET A2 antenna, shown in figure 1, includes the coaxial feeding ports, straps, septa, and Faraday screens. This CAD model represents a flattened version of the actual geometry, which in reality follows the toroidal curvature of the JET tokamak walls.

A plasma volume has been added in front of the antenna, as shown in figures 2 and 3. A vacuum region is assumed between the tokamak walls and the plasma. The plasma profiles are configured to avoid resonances that could lead to numerical instabilities [8] and difficult meaningful comparisons.

The benchmark simulations are based on two specific JET pulses: 94998 and 100187. Figures 4 and 5 show the radial electron density and magnetic field profiles for these pulses, respectively. These profiles were derived from JET diagnostic measurements [9, 10] and were used as input for both the ERMES and TOPICA simulations.

JET Pulse Number (JPN) 94998 was simulated at a frequency of f = 42.5 MHz with a $0\pi0\pi$ strap polarization and a coupled power of P = 1 MW. The plasma composition consisted of 2.5% Hydrogen (H) and 97.5% Deuterium (D). At the plasma surface directly in front of the

*Corresponding author: ruben.otin@ukaea.uk

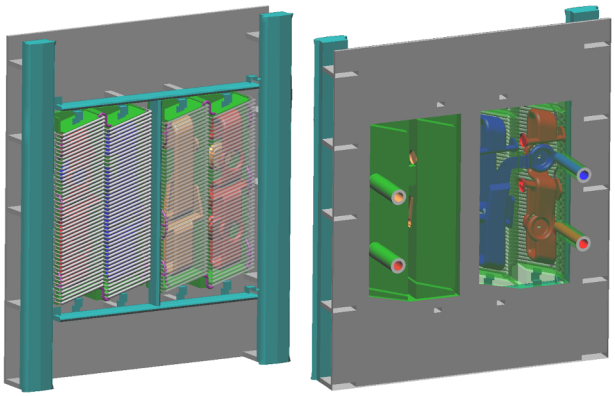

Figure 1. Three-dimensional CAD model of the JET A2 ICRF antenna used as input for both ERMES and TOPICA simulations. The model includes the coaxial feeding ports, straps, septa, and the Faraday screen.

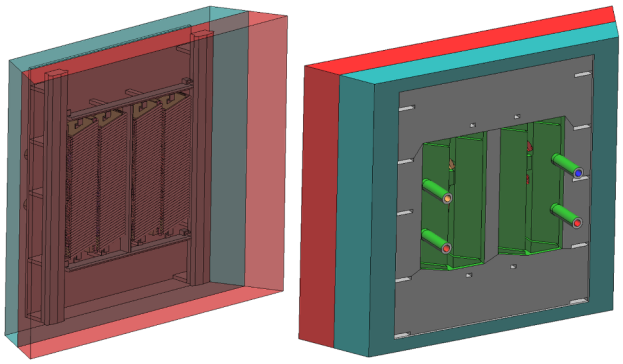

Figure 2. Simulation domain showing the JET A2 antenna and the plasma volume (in red) positioned in front of the antenna aperture.

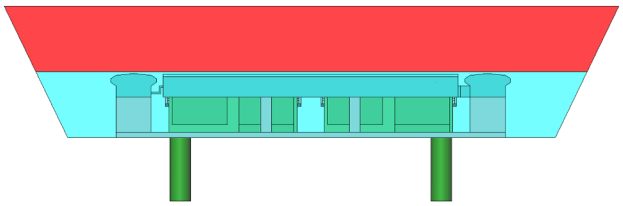

Figure 3. Top-view of the antenna–plasma system providing a clear view of the relative position of the plasma with respect to the antenna limiters.

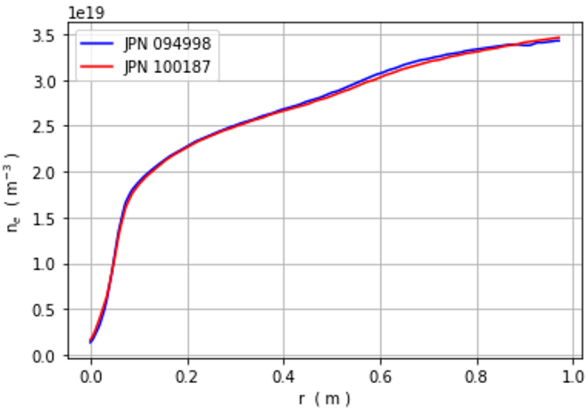

Figure 4. Electron density profiles for JET pulses 94998 and 100187. The first data point has an electron density of $n_e = 1.339 \times 10^{18}\,m^{-3}$ for JPN 94998, and $n_e = 1.617 \times 10^{18}\,m^{-3}$ for JPN 100187.

antenna, the first data point of the electron density profile is $n_e = 1.339 \times 10^{18}\,m^{-3}$, and the magnetic flux density at that location is $B = 2.257\,T$, with a angle of 8.6° relative to the antenna axis. This angle is maintained throughout the entire plasma volume.

JPN 100187 was also simulated at a frequency of $f = 42.5\,MHz$ with a $0\pi0\pi$ strap polarization. The coupled power in this case was $P = 0.5\,MW$. The plasma composition consisted of 2.5% Hydrogen (H) and 97.5% Tritium (T). The first data point at the plasma surface has an electron density of $n_e = 1.617 \times 10^{18}\,m^{-3}$ and magnetic flux density of $B = 2.286\,T$, with a angle of of 8.4° relative to the antenna axis, which is maintained throughout the entire plasma volume.

The objective of the benchmark is twofold: first, to compute the scattering matrix (S-matrix) from the four coaxial ports; and second, to use this information to normalize the electromagnetic fields for a given coupled power. Based on the antenna geometry and pulse data, the S-matrix is calculated using the approaches outlined in sections 3 and 4. The resulting S-matrix is then used to normalize the fields to the specified output power, following the methods described in [11, 12]. The normalized electromagnetic fields are compared in the same poloidal plane, located between the limiters and the Faraday screen.

3 ERMES model

ERMES 20.0 [4] is an open-source code that solves the time-harmonic Maxwell equitations with the finite element method [13]. One of its key features is the ability to choose from various FEM formulations and, for this work, we have selected the double-curl formulation with edge elements. This formulation is stated as follows: if $L^2(\Omega)$ is the Hilbert space of all the square-integrable functions in the problem domain Ω and $\mathbf{H}_0(\mathbf{curl};\Omega)$ is the functional space defined as

$$\mathbf{H}_0(\mathbf{curl};\Omega) := \{\,\mathbf{F} \in \mathbf{L}^2(\Omega) \;|\; \nabla\times\mathbf{F} \in \mathbf{L}^2(\Omega),\; \hat{\mathbf{n}}\times\mathbf{F} = 0 \;\text{ in}\;\Gamma\,\}, \tag{1}$$

where Γ is a Perfect Electric Conductor (PEC) surface. Then, solving the time-harmonic Maxwell's equation with the double-curl finite element formulation is equivalent to find an electric field $\mathbf{E} \in \mathbf{H}_0(\mathbf{curl};\Omega)$ such as $\forall\,\mathbf{F} \in \mathbf{H}_0(\mathbf{curl};\Omega)$ holds:

$$\int_\Omega \frac{1}{\mu}(\nabla\times\mathbf{E})\cdot(\nabla\times\bar{\mathbf{F}}) - \omega^2\int_\Omega \varepsilon\mathbf{E}\cdot\bar{\mathbf{F}} + \int_{\partial\Omega}\frac{1}{\mu}(\hat{\mathbf{n}}\times\nabla\times\mathbf{E})\cdot\bar{\mathbf{F}} = i\omega\int_\Omega \mathbf{J}\cdot\bar{\mathbf{F}}, \tag{2}$$

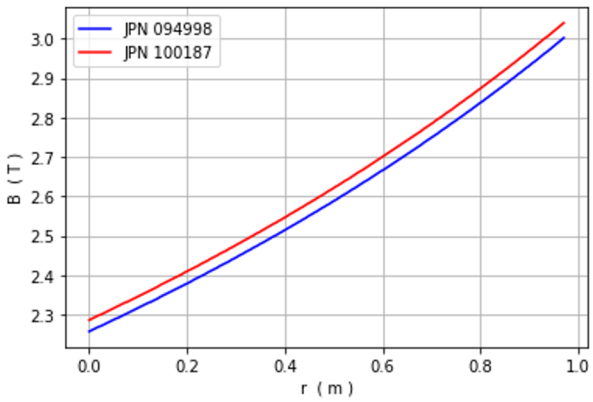

Figure 5. Magnetic flux density profiles corresponding to JET pulses 94998 and 100187. The first data point has a magnetic flux density of B = 2.257 T for JPN 94998, and B = 2.286 T for JPN 100187.

where ω is the angular frequency of the time-harmonic problem, $\mathbf{J}$ is the volumetric current source densities, $\hat{\mathbf{n}}$ is the unitary exterior normal to the problem domain Ω with boundary $\partial\Omega$, μ is the complex magnetic permeability (equal to the vacuum permeability μ_0 in this work), and ε is the cold plasma permittivity tensor defined in [15, 16].

ERMES 20.0 can continuously integrate the dielectric tensor across the problem domain; however, for this work, a discontinuous transition from vacuum to cold plasma has been considered to allow for direct comparison with TOPICA. The above formulation was discretized using second-order curl-conforming elements [14], which have 20 degrees of freedom per element. A detail of the mesh used to discretize the antenna geometry is shown in figure 6.

For the boundary conditions, ERMES 20.0 applies a PEC condition ($\hat{\mathbf{n}} \times \mathbf{E} = 0$) on the antenna structure and side surfaces, and Robin boundary conditions on the remaining surfaces (coaxial ports and the outer plasma boundary). On the input ports, the following condition is applied:

$$\hat{\mathbf{n}} \times \nabla \times \mathbf{E} - \gamma\,(\hat{\mathbf{n}} \times \hat{\mathbf{n}} \times \mathbf{E}) = -2\,\gamma\,(\hat{\mathbf{n}} \times \hat{\mathbf{n}} \times \mathbf{E}_{\mathrm{TEM}}), \quad (3)$$

where $\gamma = i\omega\sqrt{\varepsilon\mu}$ is the propagation constant of the TEM mode, with ε and μ being the permittivity and permeability of the coaxial medium, respectively, and

$$\mathbf{E}_{\mathrm{TEM}} = |E_0|e^{i\theta}\sqrt{\frac{\eta}{2\pi\ln(b/a)}}\left(\frac{e^{\gamma z}}{\mathrm{r}}\right)\hat{\mathbf{r}}, \quad (4)$$

where $|E_0|e^{i\theta}$ is a complex scale factor, $\eta = \sqrt{\mu/\varepsilon}$, a is the diameter of the inner cylinder of the coaxial waveguide, b is the diameter of the exterior cylinder of the coaxial waveguide, r is the radial coordinate and, $\hat{\mathbf{r}}$ is the unitary radial vector. On the output ports, the same boundary condition is applied, but with $\mathbf{E}_{\mathrm{TEM}} = 0$. On the outer plasma boundary, the same expression (3) also applies, again with $\mathbf{E}_{\mathrm{TEM}} = 0$, but with $\gamma = ik_0\sqrt{RL/S}$, where $k_0 = \omega\sqrt{\epsilon_0\mu_0}$ is the angular wave number in vacuum, and R, L, and S are components of the cold plasma dielectric tensor [15, 16]. These conditions correspond to the assumption that a fast wave is propagating toward the outer plasma boundary.

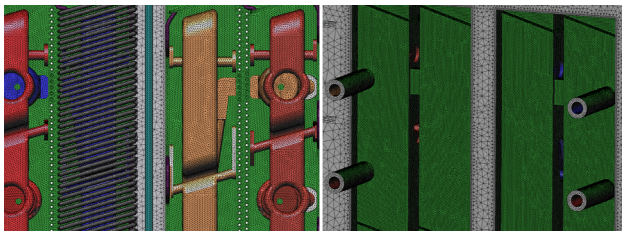

Figure 6. Details of the FEM mesh used in ERMES.

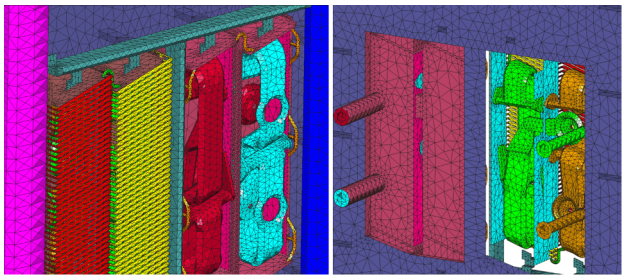

Figure 7. Details of the MoM surface mesh used in TOPICA.

In this benchmark, since cold plasma resonances are intentionally avoided by construction, it is not necessary to introduce any numerical damping into the cold plasma tensor [8].

4 TOPICA model

TOPICA [5] is a frequency-domain numerical code based on the method of moments [17], and it has become a reference tool in the fusion community for simulating the coupling between ICRH antennas and the plasma. It has been validated through applications on several devices, including JET, ASDEX Upgrade, and ITER.

TOPICA integrates the plasma self-consistently through its coupling with FELICE [18, 19], a one-dimensional finite element code that computes the plasma response. FELICE solves the wave equations in the plasma along the radial coordinate and connects with TOPICA via the spectral plasma Green's function [5], calculated at an interface separating the vacuum from the plasma. This integration enables a hybrid numerical framework: MoM is used for the antenna and vacuum region, while FEM is applied to the plasma. This approach allows for detailed simulation of power coupling, reflection coefficients, and the spatial distribution of electric fields. In addition, TOPICA supports the analysis of realistic antenna geometries, including Faraday screens, limiters, and matching circuits, making it a powerful tool for the design and optimization of ICRH systems.

For the benchmark described in section 2, the boundary conditions used by TOPICA are as follows: PEC conditions are applied to all antenna structures and side surfaces, TEM modes are imposed at the coaxial ports to excite the fields, and plasma behaviour is modeled through coupling with FELICE. Figure 7 shows the surface mesh used to discretize the antenna structure.

Table 1. Scattering parameters matrix for JPN 94998. H: 2.5%, D: 97.5%, 0π0π, f = 42.5 MHz, P = 1 MW.

	ERMES $\lvert S_{ji}\rvert \angle\theta\,(rad)$	TOPICA $\lvert S_{ji}\rvert \angle\theta\,(rad)$
S_{11}	0.8143 /+0.5006	0.7688 /+0.1041
S_{21}	0.0677 /−3.0302	0.0641 /+2.6696
S_{31}	0.0664 /−2.9264	0.0328 /+2.5035
S_{41}	0.0767 /+3.1230	0.0428 /+2.3693
S_{12}	0.0736 /−3.0116	0.0664 /+2.6557
S_{22}	0.8691 /+1.3146	0.8469 /−0.8902
S_{32}	0.0509 /−2.6014	0.0271 /+2.5141
S_{42}	0.0626 /−2.8309	0.0314 /+2.3424
S_{13}	0.0639 /−2.8807	0.0350 /+2.2106
S_{23}	0.0472 /−2.5499	0.0227 /+2.2743
S_{33}	0.8718 /+1.3164	0.8545 /−0.9096
S_{43}	0.0520 /−2.5567	0.0668 /+2.2524
S_{14}	0.0827 /−3.0581	0.0546 /+2.1546
S_{24}	0.0592 /−2.8005	0.0349 /+2.0127
S_{34}	0.0573 /−2.4980	0.0712 /+2.1960
S_{44}	0.8118 /+0.4620	0.7702 /+0.1107

Table 2. Scattering parameters matrix for JPN 100187. H: 2.5%, T: 97.5%, 0π0π, f = 42.5 MHz, P = 0.5 MW.

	ERMES $\lvert S_{ji}\rvert \angle\theta\,(rad)$	TOPICA $\lvert S_{ji}\rvert \angle\theta\,(rad)$
S_{11}	0.8201 /+0.4963	0.7638 /+0.1015
S_{21}	0.0671 /+3.0678	0.0676 /+2.6995
S_{31}	0.0605 /−3.0751	0.0376 /+2.3463
S_{41}	0.0741 /+2.9759	0.0558 /+2.2967
S_{12}	0.0700 /+3.0965	0.0665 /+2.7930
S_{22}	0.8732 /+1.3119	0.8416 /−0.8887
S_{32}	0.0502 /−2.7664	0.0265 /+2.3166
S_{42}	0.0563 /−2.9944	0.0368 /+2.1557
S_{13}	0.0658 /−2.9450	0.0374 /+2.6657
S_{23}	0.0485 /−2.6847	0.0318 /+2.6040
S_{33}	0.8751 /+1.3116	0.8492 /−0.9074
S_{43}	0.0455 /−2.7108	0.0723 /+2.2332
S_{14}	0.0810 /+3.0708	0.0462 /+2.5803
S_{24}	0.0626 /−2.8481	0.0357 /+2.5401
S_{34}	0.0464 /−2.6438	0.0665 /+2.3710
S_{44}	0.8168 /+0.4539	0.7650 /+0.1084

5 Validation results

The objective of the benchmark is first, to compute the scattering matrix from the four coaxial ports and second, to use this matrix to normalize the electromagnetic fields for a specified output power and to visualize the resulting fields in a poloidal plane near the antenna. These calculations are performed using the antenna geometry, pulse data, and numerical models described in the preceding sections.

Tables 1 and 2 show the computed scattering parameters obtained from both simulation tools for JPN 94998 and JPN 100187, respectively. The scattering matrix elements are expressed as S_{ji}, where the indices j and i correspond to each of the four coaxial ports of the JET A2 antenna. A good level of agreement is observed between ERMES and TOPICA, indicating consistency in the treatment of port excitations and boundary conditions across the two numerical approaches.

To compute the electromagnetic fields, TOPICA imposes a voltage of 1 V (through a TEM mode) at each port, with a phase shift of 25° applied to ports 1 and 4 to account for the approximate 50 cm difference in the feeding line lengths. This results in the following complex voltage excitations: $V_1^t = 0.9063 - i\,0.4226$, $V_2^t = -1.0$, $V_3^t = 1.0$, and $V_4^t = -0.9063 + i\,0.4226$, which correspond to the desired $0\pi0\pi$ strap excitation pattern. Using these voltages along with the computed scattering matrix, the net power delivered to the plasma is calculated using the formula [11]:

$$P_{\text{tot}} = \frac{1}{2Z_0} \sum_{j=1}^{4} \left(|V_j^f|^2 - |V_j^b|^2 \right), \tag{5}$$

where $Z_0 = 30\,\Omega$ is the characteristic impedance of the coaxial ports, V_j^f is the forward voltage at port j, and V_j^b is the corresponding backward voltage. The forward and backward voltage vectors are computed from the total applied voltages $\mathbf{V}^t$ using the expressions [11]:

$$\mathbf{V}^f = [\,\mathbf{S} + \mathbf{U}\,]^{-1} \cdot \mathbf{V}^t, \tag{6}$$

$$\mathbf{V}^b = \mathbf{S} \cdot \mathbf{V}^f, \tag{7}$$

where $\mathbf{S}$ is the scattering matrix and $\mathbf{U}$ is the identity matrix. Finally, the normalization constant α used to scale the fields to a desired output power P_0 is given by:

$$\alpha = \sqrt{\frac{P_0}{P_{\text{tot}}}}. \tag{8}$$

ERMES follows a similar procedure, with the primary difference being that the voltage excitations in TOPICA must be translated into the electric field values used in the boundary condition (3). To achieve this, we use the same complex voltage vector $\mathbf{V}^t$ imposed in TOPICA and apply the relation $|E_0|e^{i\theta} = V^f/\sqrt{Z_0}$ in (4). We then use equations (5) through (8), replacing $\mathbf{S}$ with the scattering matrix computed by ERMES, to calculate the normalization factor α. This approach ensures that the boundary conditions in ERMES accurately reproduce the desired excitation at the coaxial ports, allowing for a consistent comparison between the two simulation frameworks. The normalized fields obtained from this procedure are shown in figures 8, 9, 10, and 11. These figures demonstrate excellent agreement between the results produced by both simulation tools, thereby validating the accuracy of the ERMES approach for modeling ICRH antenna–plasma interactions.

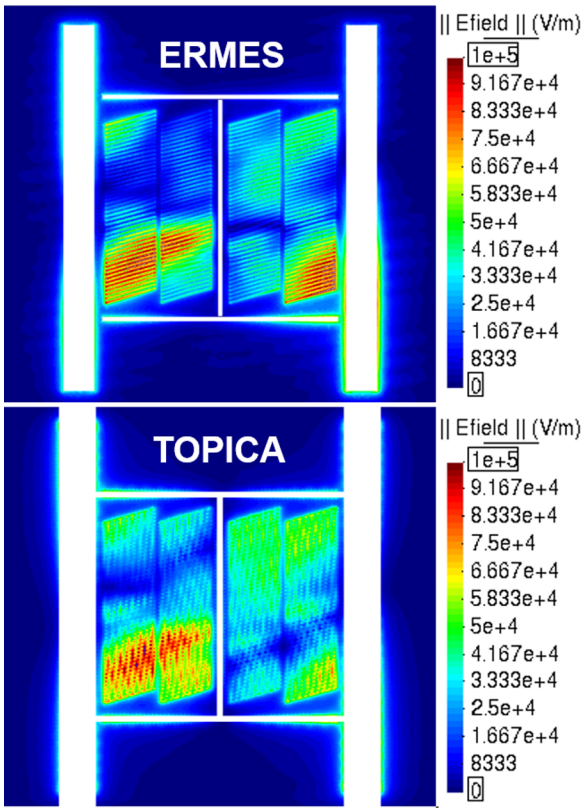

Figure 8. Magnitude of the electric field in a plane located between the plasma and the Faraday screen for JPN 94998.

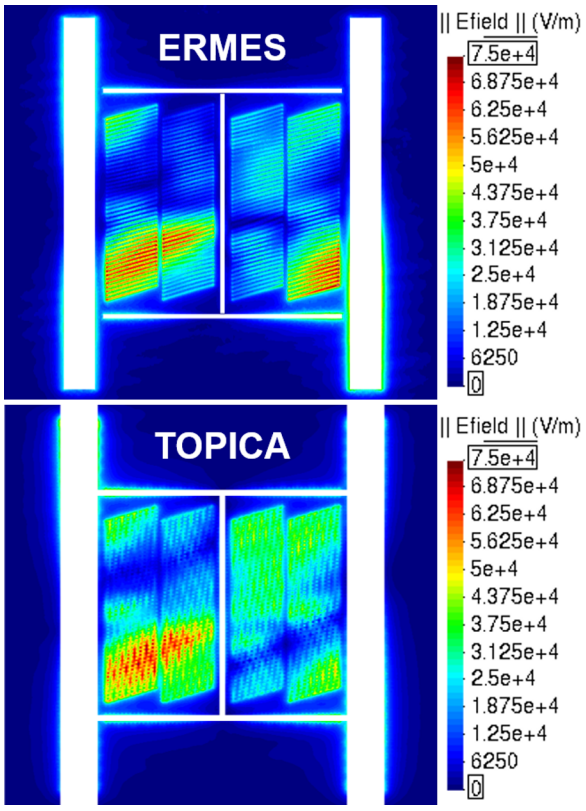

Figure 10. Magnitude of the electric field in a plane located between the plasma and the Faraday screen for JPN 100187.

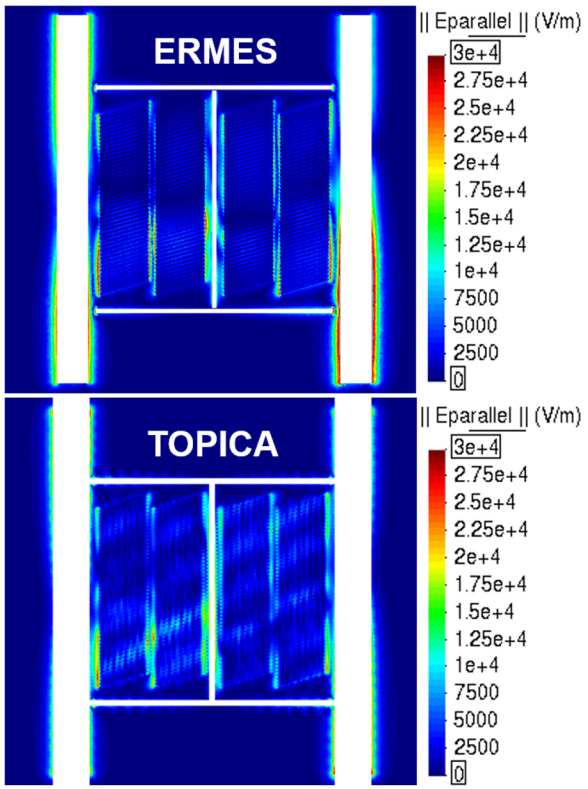

Figure 9. Magnitude of the electric field component parallel to the tokamak magnetic flux density in a plane located between the plasma and the Faraday screen for JPN 94998.

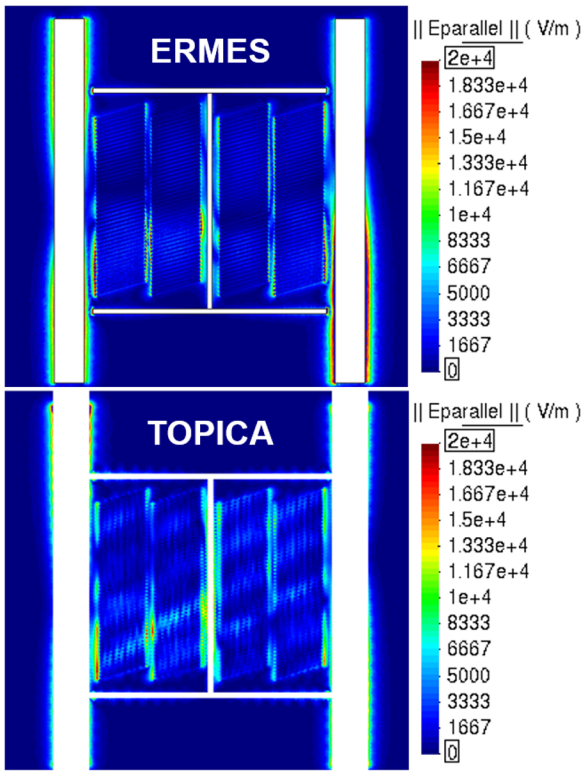

Figure 11. Magnitude of the electric field component parallel to the tokamak magnetic flux density in a plane located between the plasma and the Faraday screen for JPN 100187.

6 Summary

This study presents a validation of the finite element code ERMES 20.0, benchmarked against the well-established method of moments code TOPICA. The benchmark focuses on ICRH coupling for a JET A2 antenna, comparing key outputs such as the scattering matrix and the electromagnetic fields in the vicinity of the antenna.

The results demonstrate excellent agreement between the two codes, confirming the accuracy and robustness of the finite element approach adopted by ERMES 20.0. This agreement underscores its suitability for modeling complex antenna–plasma interactions in fusion environments, including phenomena critical to ICRH performance such as wave coupling efficiency and sheath rectification.

Beyond validation, the analysis highlights the flexibility and extensibility of ERMES 20.0, positioning it as a promising tool for future studies. Planned developments include the integration of warm and hot plasma effects, and non-linear boundary models, with the aim of enhancing predictive modeling for next-generation fusion devices.

References

[1] J. Hillairet, Review on recent progress in ion cyclotron range of frequency systems, experiments and modelling for magnetic confinement fusion, Rev. Mod. Plasma Phys. **7**, 16 (2023). https://doi.org/10.1007/s41614-023-00116-5

[2] J. Ongena et al., Recent advances in physics and technology of ion cyclotron resonance heating in view of future fusion reactors, Plasma Phys. Control. Fusion **59**, 054002 (2017). https://doi.org/10.1088/1361-6587/aa5a62

[3] V. Bobkov et al., Impact of ICRF on the scrape-off layer and on plasma wall interactions: From present experiments to fusion reactor, Nucl. Mater. Energy **18**, 131-140 (2019). http://doi.org/10.1016/j.nme.2018.11.017

[4] R. Otin, ERMES 20.0: Open-source finite element tool for computational electromagnetics in the frequency domain, Comput. Phys. Commun. **310**, 109521 (2025). https://doi.org/10.1016/j.cpc.2025.109521

[5] D. Milanesio et al., A multi-cavity approach for enhanced efficiency in TOPICA RF antenna code, Nuclear Fusion **49**(11), 115019 (2009). https://doi.org/10.1088/0029-5515/49/11/115019

[6] A. Kaye et al., Present and future JET ICRF antennae, Fusion Eng. Des. **24**(1), 1-21 (1994). https://doi.org/10.1016/0920-3796(94)90034-5

[7] I. Monakhov et al., Assessment of the JET ICRH system performance since 2000, Plasma Phys. Control. Fusion **67**, 015023 (2025). https://doi.org/10.1088/1361-6587/ad9e73

[8] R. Otin et al., Full wave simulation of RF waves in cold plasma with the stabilized open-source finite element tool ERMES, AIP Conf. Proc. **2254**, 050009 (2020). https://doi.org/10.1063/5.0013549

[9] A. Sirinelli et al., Multiband reflectometry system for density profile measurement with high temporal resolution on JET tokamak, Rev. Sci. Instrum. **81**, 10D939 (2010). https://doi.org/10.1063/1.3502329

[10] A. Boboc et al., Upgrade of the JET far infrared interferometer diagnostic, Rev. Sci. Instrum. **83**, 10E341 (2012). https://doi.org/10.1063/1.4737420

[11] D. M. Pozar, Microwave Engineering (John Wiley & Sons, Hoboken, 2012).

[12] I. Monakhov et al., ICRH antenna S-matrix measurements and plasma coupling characterisation at JET, Nucl. Fusion **58**, 046012 (2018). https://doi.org/10.1088/1741-4326/aaace3

[13] J. Jin, The finite element method in electromagnetics (John Wiley & Sons, Hoboken, 2014).

[14] M. Salazar-Palma et al., Iterative and self-adaptive finite-elements in electromagnetic modeling (Artech House, Boston, 1998).

[15] T. H. Stix, Waves in plasmas (Springer-Verlag, New York, 1992).

[16] D. G. Swanson, Plasma waves (Academic press, London, 1989).

[17] R. F. Harrington, Field computation by moment methods (John Wiley & Sons, Hoboken, 1992).

[18] M. Brambilla, Finite Larmor radius wave equations in tokamak plasmas in the ion cyclotron frequency range, Plasma Phys. Control. Fusion **31**, 723 (1989). https://doi.org/10.1088/0741-3335/31/5/004

[19] V. Lancellotti et al., TOPICA: an accurate and efficient numerical tool for analysis and design of ICRF antennas, Nucl. Fusion **46**, S476 (2006). https://doi.org/10.1088/0029-5515/46/7/S10